Threshold of hierarchical percolating systems

Jiantong Li,[1] Biswajit Ray,[2] Muhammad A. Alam,[2,*] and Mikael Östling[1]

[1]*KTH Royal Institute of Technology, School of Information and Communication Technology, Electrum 229, SE-164 40 Kista, Sweden*

[2]*School of Electrical and Computer Engineering, Purdue University, West Lafayette, Indiana 47907-1285, USA*

(Received 2 September 2011; revised manuscript received 27 December 2011; published 7 February 2012)

Many modern nanostructured materials and doped polymers are morphologically too complex to be interpreted by classical percolation theory. Here, we develop the concept of a hierarchical percolating (percolation-within-percolation) system to describe such complex materials and illustrate how to generalize the conventional percolation to double-level percolation. Based on Monte Carlo simulations, we find that the double-level percolation threshold is close to, but definitely larger than, the product of the local percolation thresholds for the two enclosed single-level systems. The deviation may offer alternative insights into physics concerning infinite clusters and open up new research directions for percolation theory.

DOI: 10.1103/PhysRevE.85.021109 PACS number(s): 64.60.ah

I. INTRODUCTION

Over the last half century since its introduction, percolation theory has become an increasingly sophisticated field with broad applications in phase transition [1], conduction through random network [2], polymer physics [3], etc., with a high degree of confidence in its key predictions of thresholds, critical exponents, and scaling relationship. The research interest has broadened from classical percolation on regular lattices [3], to continuum percolation on networks (irregular lattices) [4,5], to complicated percolation on specialized lattices [6,7], to recent explosive percolation [8]. Even so, the existing theoretical analyses are typically dedicated to single-level percolation (SLP) systems, which are composed of sites or bonds as the most primary elements.

In practice, however, percolation occurs in a broader class of physical systems than those typically considered in classical literature of SLP theory. For example, percolation-like phenomena could arise in systems where each element (site, bond, etc.) *itself* is comprised of another (finer grain) independent percolation system, such that the occupied elements are further populated by certain sub-elements. Such *percolation-within-percolation* systems are widely, and probably were first, found in conductive polymer blends [9,10]. Phase separation takes place in the blend of conducting polymer (CP) and matrix polymer to form CP-rich phases, which compose the first-level percolation. Within a CP-rich phase, the CP forms the second-level percolation. We propose to name the hierarchical systems as double-level percolation (DLP), or in general, multilevel percolation (MLP) when more than two levels are involved in the hierarchy [11]. Today, DLP is not limited to polymer science, but a wide variety of nanomaterials offer rich collection for DLP. For example, the recently introduced hierarchical mesoporous molecule sieves [12] actually construct DLP systems, where the porous nanoparticles form the first-level percolation, while within each nanoparticle, pores constitute the second-level percolation. Another example might be graphene thin films [13,14], where the network of a large number of graphene flakes forms the first-level percolation, and meanwhile each graphene flake can be modeled as a random resistor network (the second-level percolation) of electron and hole puddles [15].

Despite the increasing interest of DLP in practice, so far, little theoretical work has been done to study these systems systematically. Here, we offer such a perspective to this emerging class of percolation problems.

II. MODELING AND PROCEDURE

In general, a DLP comprises an upper-level lattice, each of whose elements [sites or bonds for (regular) lattice; disks, sticks, etc., for network (irregular lattice)] hierarchically comprises an independent lower-level lattice. All the lower-level lattices are identical, but can be different from the upper-level one. For clarity, the elements in the upper- and lower-level lattices are named with prefixes "super" and "sub," respectively. As an example, in this section, we discuss in detail a two-dimensional (2D)-bond:2D-bond DLP (illustrated in Fig. 1), where both the upper-level system (of size L_1) and the lower-level systems (of size L_2) involve 2D bond percolation on square lattice [3]. Later, we will also extend the discussion to the 2D-bond:2D-site (Sec. III B) and one-dimensional (1D)-bond:2D-bond (Sec. III C) DLP systems.

In the 2D-bond:2D-bond DLP system, each lower-level lattice [Fig. 1(b)] corresponds to a super-bond in the upper-level lattice [Fig. 1(a)], and has its own local boundaries, one (opposite) pair of which connect the super-sites (filled green squares in Fig. 1; all super-sites are occupied), so that all the lower-level lattices are independent from one another. The most significant feature which distinguishes DLP from SLP is that the population process in DLP comprises two sequential steps: First, a fraction of super-bonds are randomly chosen as occupied [blue bold bonds in Fig. 1(a)]; and then, sub-bonds are uniformly deposited *only* on those lower-level lattices corresponding to *occupied* super-bonds [referring to Fig. 1(b); only those lower-level lattice with cyan background can be populated by occupied sub-bonds (dark red bonds)]. The DLP percolates when the occupied sub-bonds (together with super-sites) can form continuous path(s) connecting two opposite global boundaries [vertical black bold lines at the leftmost and rightmost edges in Fig. 1(b)]. The fraction of occupied sub-bonds with respect to *all* the N sub-bonds in the DLP ($N = 4L_1^2L_2^2$ in Fig. 1) is called *global* occupation

*alam@purdue.edu

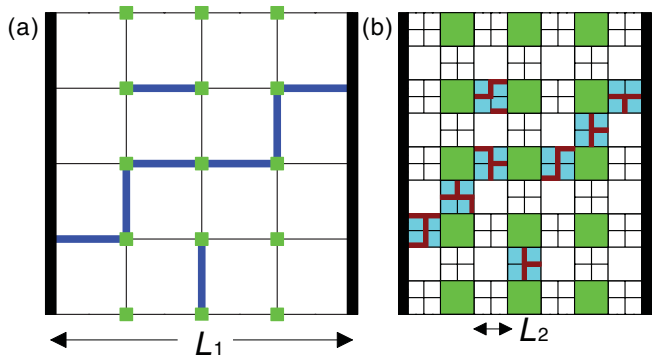

FIG. 1. (Color online) Lattice of the 2D-bond:2D-bond DLP. (a) The upper-level lattice (of size $L_1 = 4$) with some occupied super-bonds (blue bold lines). (b) The overall DLP lattice with some occupied sub-bonds (dark red bold lines). Each lower-level lattice (of size $L_2 = 2$) corresponds to a super-bond in (a). Only those lower-level lattices (shaded cyan) which correspond to occupied super-bonds can be populated by sub-bonds. The filled green squares in both (a) and (b) are occupied super-sites, which connect super-bonds [in (a)] or the local boundaries of lower-level lattices [in (b)]. The global DLP boundaries (vertical black bold lines) in (b) are also the upper-level lattice boundaries in (a).

probability and denoted as p. The fraction of occupied super-bonds (sub-bonds) with respect to the $2L_1^2$ super-bonds ($2L_2^2$ sub-bonds) in the upper-level (lower-level) lattice is called *local* occupation probability and denoted as p_1 (p_2). We will now calculate the *global* percolation threshold p_c, a key parameter for the hierarchical percolation problem.

In SLPs, an effective way to measure the percolation threshold is first estimating p_c as $p_{\text{est}}(L)$ for different system sizes L based on spanning probability function $R(p, L)$, and then converging these estimates to the true p_c using finite-size scaling with proper correction terms [5,16–19]. The function $R(p, L)$ gives the probability that a continuous path spans (bridges) the system from one boundary to another at occupation probability p and system size L. In general, one can adopt the fixed-spanning-probability estimates $p_\tau(L)$, defined by $R(p_\tau, L) = \tau$ with τ as an arbitrary constant within $0 < \tau < 1$, and extract p_c from a previously proposed general form [18] as

$$p_\tau(L) - p_c = \sum_{k=0}^{M} A_k(\tau) L^{-(k+1/\upsilon)}, \tag{1}$$

where υ is critical correlation-length exponent [3], and $A_k(\tau)$ are τ-dependent coefficients. For faster convergence, the cell-to-cell estimates $p_{c-c}(L)$, defined by $R(p_{c-c}, L) = R(p_{c-c}, L/2)$, may be used, and p_c can be extracted from the following equation [19]:

$$p_{c-c}(L) - p_c = \sum_{k=1}^{M'} c_k L^{-(k+1/\upsilon)}, \tag{2}$$

where c_k are system-dependent coefficients.

In the present work, these SLP-specific methodologies must be generalized for DLPs. First, we determine the generalized spanning probability function $R(p,L_1,L_2)$ of, for example, the 2D-bond:2D-bond DLP. Here $R(p,L_1,L_2)$ gives the probability that a DLP spans (percolates) at the global occupation probability p, the upper-level system size L_1 and the lower-level system size L_2. We start with a blank upper-level square lattice. Then the super-bonds are filled randomly until the upper-level system spans for the first time [referring to Fig. 1(a), until a continuous path of super-bonds first bridges the left and right boundaries]. The number of the occupied super-bonds is recorded as N_1. Specially, those super-bonds attached to the backbone of a percolating cluster are marked, and their number is recorded as N_b. Afterwards, tokens are generated and each token is randomly allocated to one of the N_1 occupied super-bonds except those that are already of full ($2L_2^2$) tokens. When a super-bond embedded in the *backbone* get a token, a sub-bond is generated to populate the corresponding lower-level lattice [20]. Since none of the N_1-N_b nonbackbone super-bonds (though occupied) can really contribute to the DLP spanning, it is not necessary to populate their lower-level lattices. We repeatedly generate the tokens until the DLP spans through sub-bonds for the first time. The total token number n_f represents the minimum sub-bond number needed for the DLP spanning for one simulation run, which results in one step function Θ_n, as $\Theta_n = 0$ for $n < n_f$ and $\Theta_n = 1$ for $n \geqslant n_f$. After repeating the simulations for m runs, we obtain $R(p,L_1,L_2)$ by the following three-step process: (i) Superimpose all the m step functions Θ_n, (ii) divide the results by mN, and (iii) convolve them with a binomial distribution to get the "canonical ensemble" of $R(p,L_1,L_2)$ for any arbitrary value of p [16–18].

Currently, however, there is no analog of Eqs. (1) and (2) for precise estimation of the percolation threshold for the infinite DLP system ($L_1 \to \infty$ and $L_2 \to \infty$). Obviously, the full generalization of Eqs. (1) and (2) is expected to be more complicated since they should depend on both L_1 and L_2, as well as their interactions. Nevertheless, a simple approach to infinite DLPs (that can still use the SLP algorithm) involves the following idea: We consider a set of finite systems where L_1 is proportional to L_2, that is, $L_1 = bL_2$ with b a constant. If we set $L_2 \equiv L$ (or $L_1 \equiv L$), then $L_1 = bL$ (or $L_2 = L/b$). Therefore, once $L \to \infty$, both $L_1 \to \infty$ and $L_2 \to \infty$ simultaneously, and the global p_c for the DLP can be determined by asymptotic extrapolation.

III. RESULTS

On the basis of the algorithm above, we investigate the global percolation threshold for three kinds of DLPs. In this work, all the upper- and lower-level percolations are characterized by free boundary conditions, and each data point is typically based on $10^4 - 10^7$ simulation samples.

A. 2D-bond:2D-bond DLP

We first study the 2D-bond:2D-bond DLP, as illustrated in Fig. 1. Figure 2 shows the simulated spanning probability functions. According to Eq. (1), if one plots $p_\tau(L)$ against $L^{1/\upsilon}$ for different τ, all the data should converge to p_c when $L \to \infty$. Figures 3(a)–3(c) display such plots for three types of $p_\tau(L)$ respectively defined by the following: (i) $R(p_{\tau,1},L,L) = \tau$, where $L_1 = L_2 = L$; (ii) $R(p_{\tau,2},L/2,L) = \tau$, where $2L_1 = L_2 = L$; and (iii) $R(p_{\tau,3},L,L/2) = \tau$, where $L_1 = 2L_2 = L$. In all plots, τ varies from 0.1 to 0.9 but all the data can

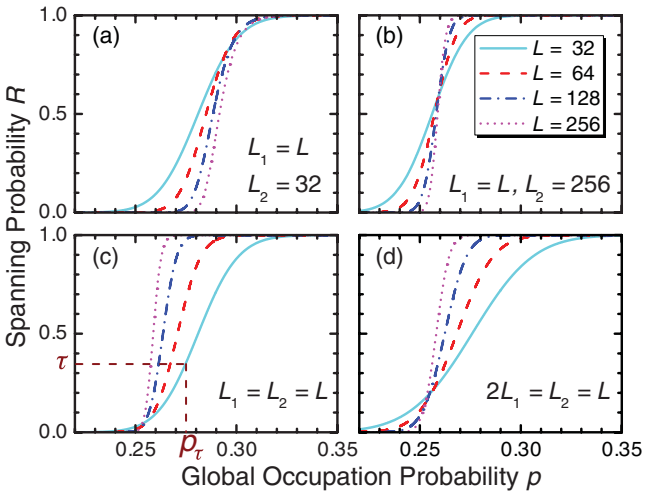

FIG. 2. (Color online) Simulated spanning probability function $R(p,L_1,L_2)$ for the 2D-bond:2D-bond DLP with different system sizes. (a) $L_2 = 32$ and (b) $L_2 = 256$ are fixed while L_1 varies. (c) $L_1 = L_2 = L$ and (d) $2L_1 = L_2 = L$. In (c), the dashed lines indicate how the percolation threshold estimate p_τ is calculated.

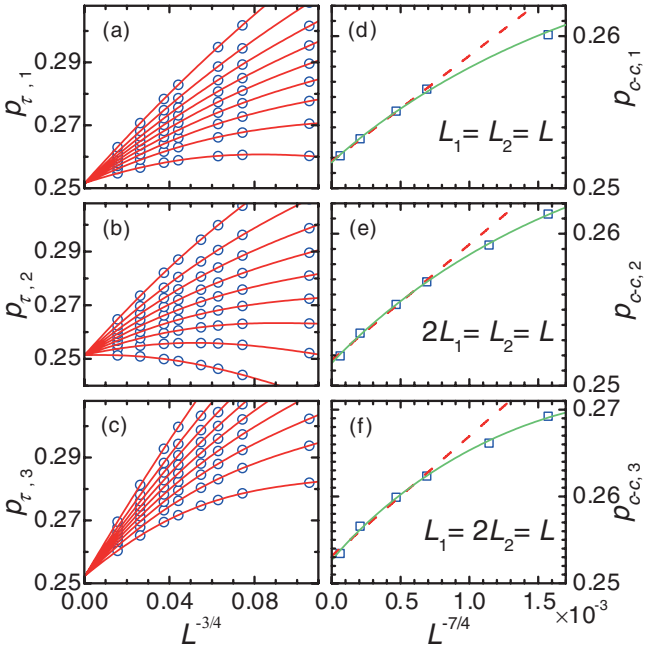

FIG. 3. (Color online) Finite-size scaling of p_c estimates for the 2D-bond:2D-bond DLP. (a)–(c) Plots of the three types of fixed-spanning-probability estimates $p_\tau(L)$ against $L^{-1/\upsilon}$ for different τ. The curves are nonlinear regression fittings by Eq. (1) with $M = 2$ and $\upsilon = 4/3$. In each plot, from bottom to top, τ increases from 0.1 to 0.9 in steps of 0.1. (d)–(f) Plots of the three types of cell-to-cell estimates $p_{c-c}(L)$ against $L^{-1-1/\upsilon}$. The dashed lines are linear fittings by Eq. (2) (with $M' = 1$) to the leftmost four data points ($L = 64$, 80, 128, and 256), and the solid curves are nonlinear regression fittings by Eq. (2) (with $M' = 2$) to all the plotted data.

be well fitted (adjusted $R^2 > 0.999$) by Eq. (1) with $M = 2$ and $\upsilon = 4/3$. Note that the critical correction-length exponent here is still $\upsilon = 4/3$, identical to that of 2D SLP [3]. It is also clear that all these curves exhibit excellent convergences when $L\to\infty$, justifying that Eq. (1) still applies for 2D DLPs. The convergent points are listed in Table I. Moreover, as shown in Figs. 3(a)–3(c), all the convergent points in the three plots agree very well with one another, implying that the convergent points are indeed the true percolation threshold p_c.

In addition, we also investigate three types of cell-to-cell estimates $p_{c-c}(L)$, as respectively defined by the following: (i) $R(p_{c-c,1},L,L) = R(p_{c-c,1},L/2,L/2)$, where $L_1 = L_2 = L$; (ii) $R(p_{c-c,2},L/2,L) = R(p_{c-c,2},L/4,L/2)$, where $2L_1 = L_2 = L$; and (iii) $R(p_{c-c,3},L,L/2) = R(p_{c-c,3},L/2,L/4)$, where $L_1 = 2L_2 = L$. In terms of Eq. (2), the three kinds of cell-to-cell estimates p_{c-c} are plotted against $L^{-1-1/\upsilon}$ in Figs. 3(d)–3(f), respectively. It is clear that all the data can be well fitted by Eq. (2). As shown by the dashed lines, when $L\geqslant 64$ [the leftmost four points in Figs. 3(d)–3(f)], all the plots are linear and only $M' = 1$ is required in Eq. (2). When smaller L is involved, higher order corrections ($M' = 2$) are required. The regression fittings are analyzed in detail in Table II. All these p_c estimations coincide with those convergent points in Figs. 3(a)–3(c). Because of the robust convergence and small uncertainty of the linear fitting in Fig. 3(d), we take its intercept as our best estimation for the percolation threshold of the 2D-bond:2D-bond DLP. It is given by

$$p_c = 0.251\,77 \pm 0.000\,31. \tag{3}$$

TABLE I. Extracted p_c for the 2D-bond:2D-bond DLP from the nonlinear fittings ($M = 2$) of Eq. (1) to different types of p_τ in Figs. 3(a)–3(c). All the fittings have adjusted $R^2 > 0.999$.

	p_c		
τ	From $p_{\tau,1}$ [Fig. 3(a)]	From $p_{\tau,2}$ [Fig. 3(b)]	From $p_{\tau,3}$ [Fig. 3(c)]
0.1	0.25158(37)	0.25139(19)	0.25222(31)
0.2	0.25152(45)	0.25153(22)	0.25222(31)
0.3	0.25147(44)	0.25145(31)	0.25223(32)
0.4	0.25149(38)	0.25141(31)	0.25222(34)
0.5	0.25150(36)	0.25135(39)	0.25219(35)
0.6	0.25147(32)	0.25133(52)	0.25215(36)
0.7	0.25141(38)	0.25137(44)	0.25208(42)
0.8	0.25137(35)	0.25139(43)	0.25206(35)
0.9	0.25154(20)	0.25135(54)	0.25201(42)

TABLE II. Regression fittings of different p_{c-c} in Figs. 3(d)–3(f) by Eq. (2).

Data	M' in Eq. (2)	p_c	Adjusted R^2
$p_{c-c,1}$ ($L \geqslant 64$) [Fig. 3(d)]	1	0.25177(31)	0.998
$p_{c-c,2}$ ($L \geqslant 64$) [Fig. 3(e)]	1	0.25169(88)	0.989
$p_{c-c,3}$ ($L \geqslant 64$) [Fig. 3(f)]	1	0.25316(252)	0.971
$p_{c-c,1}$ (all L) [Fig. 3(d)]	2	0.25169(51)	0.998
$p_{c-c,2}$ (all L) [Fig. 3(e)]	2	0.25148(39)	0.999
$p_{c-c,3}$ (all L) [Fig. 3(f)]	2	0.25265(122)	0.996

In this work, unless specified otherwise, all uncertainty represents the 95% confidence intervals from regression analysis.

B. 2D-bond:2D-site DLP

Using the approach discussed above, we now consider as the second illustrative example the 2D-bond:2D-site DLP, whose upper- and lower-level systems are 2D bond percolation on square lattice and 2D site percolation on square lattice, respectively. The simulated threshold estimates p_τ are plotted in Fig. 4 for the case of $L_1 = L_2 = L$. Once again, we find that the data are well represented by Eq. (1) (adjusted $R^2 > 0.999$) and all estimates of $p_\tau(L)$ converge to a single point [see Fig. 4(a)]. The convergent points are listed in Table III.

For an independent estimation of the threshold based on Eq. (2), Fig. 4(b) plots the cell-to-cell estimates $p_{c-c}(L)$ against $L^{-1-1/\nu}$. As the system size increases ($L = 128$, 160, and 256), the data begin to show excellent linearity. The linear fitting (adjusted $R^2 = 0.9994$) indicates that the intercept is 0.2975(5), consistent with the convergent points in Fig. 4(a). Again, due to the robust convergence in Fig. 4(b), we take the intercept as our best estimation of p_c for the 2D-bond:2D-site DLP and it is given by

$$p_c = 0.2975 \pm 0.0005. \quad (4)$$

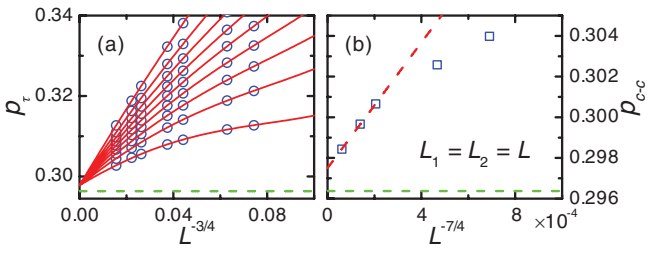

FIG. 4. (Color online) Finite-size scaling of p_c estimates for the 2D-bond:2D-site DLP with $L_1 = L_2 = L$. Each data point is based on $10^4 - 10^7$ simulation samples. (a) Plots of the fixed-spanning-probability estimates $p_\tau(L)$ against $L^{-1/\nu}$ for different τ. The curves are nonlinear regression fittings by Eq. (1) with $M = 2$ and $\nu = 4/3$. From bottom to top, τ increases from 0.1 to 0.9 in steps of 0.1. (b) Plot of cell-to-cell estimates $p_{c-c}(L)$ against $L^{-1-1/\nu}$. The dashed red line is the linear fitting by Eq. (2) (with $M' = 1$) to the leftmost three data points ($L = 128$, 160, and 256). In both (a) and (b), the horizontal dashed green lines show the value given by $p_{c1}p_{c2} = 0.5 \times 0.59274621 = 0.296373105$.

C. 1D-bond:2D-bond DLP

Finally, as shown in Fig. 5, we study a special DLP, where the upper level involves bond percolation on a line-like 1D lattice, and the lower level involves bond percolations on a 2D square lattice. Monte Carlo simulations of the percolation problem on this DLP were conducted using the same algorithm discussed in Sec. II. The only difference is that since $p_c = 1$ for any 1D lattice, we do not need to perform simulations to choose randomly the occupied super-bonds. Instead, $N_1 = N_b = L_1$ is employed for all the simulation runs. The fixed-spanning-probability estimates p_τ for systems with $L_1 = L_2 = L$ are plotted in Fig. 6. Once again, Eq. (1) fits the data very well, with adjusted $R^2 > 0.9999$. The extracted p_c (convergent points) are listed in Table IV. Although we could not calculate the cell-to-cell estimates for this 1D-bond:2D-bond DLP, we find that the convergent points in Fig. 6, as well as all the data in Table IV, are robust and clearly consistent with one another. We use the average value in Table IV to represent our best estimation of the percolation threshold as

$$p_c = 0.5022 \pm 0.0008. \quad (5)$$

Here the uncertainty brackets the maximum uncertainties of p_c estimation summarized in Table IV.

Note that this kind of DLPs can also be thought of as elongated SLPs [21,22], i.e., SLPs with a different aspect ratio $r > 1$ (in this work, $r = L_1$). However, there is a slight, but nontrivial, difference between DLPs and elongated SLPs. At infinity, for DLPs, one expects both $L_1 \to \infty$ and $L_2 \to \infty$, while for elongated SLPs, one only expects $L_2 \to \infty$, but r (or L_1) to remain fixed at a finite value. In order to demonstrate this essential difference, we use the same program to simulate the elongated SLPs (i.e., L_1 is fixed). We studied two sets

TABLE III. Extracted p_c for the 2D-bond:2D-site DLP from the nonlinear fitting ($M = 2$) of Eq. (1) to different p_τ in Fig. 4(a). All the fittings have adjusted $R^2 > 0.999$.

τ	p_c
0.1	0.29781(86)
0.2	0.29780(66)
0.3	0.29781(70)
0.4	0.29786(66)
0.5	0.29785(67)
0.6	0.29788(60)
0.7	0.29792(37)
0.8	0.29790(25)
0.9	0.29783(19)

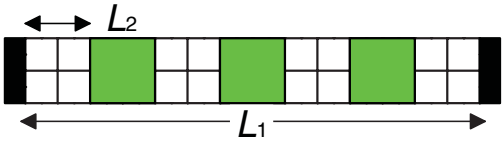

FIG. 5. (Color online) Lattice of the 1D-bond:2D-bond DLP. Big green squares are occupied super-sites. The vertical black bold lines are the global boundaries. In this figure, $L_1 = 4$ and $L_2 = 2$.

of elongated SLPs with $L_1 = 2$ and $L_1 = 256$, respectively. The simulated threshold estimates p_τ are plotted in Fig. 7. For $L_1 = 2$ [Fig. 7(a)], the data are based on $10^6 - 2 \times 10^7$ simulation samples, while for $L_1 = 256$ [Fig. 7(b)], the data are based on $10^4 - 3 \times 10^6$ simulation samples. Even linear regression, i.e., Eq. (1) with $M = 0$ and $v = 4/3$, can give excellent fit (all adjusted $R^2 > 0.999$, but actually most adjusted $R^2 > 0.99999$) to these data. As shown in Fig. 7, within the statistical errors, the elongated SLP has the same $p_c = 0.5$ as a normal SLP ($r = 1$). Note that this value for elongated SLP, however, is different from that of Eq. (5) for 1D-bond:2D-bond DLP. This distinction highlights the intrinsic difference between SLPs and DLPs.

IV. DISCUSSION

It is interesting to note that for the 2D-bond:2D-bond DLP, the local percolation thresholds for the upper- and lower-level systems (when considered independently) are both 0.5, i.e., $p_{c1} = p_{c2} = 0.5$. Then the global p_c [Eq. (3)] is very close to the product of the two local percolation thresholds ($p_{c1}p_{c2} = 0.25$). Indeed, an earlier work [10] did posit that $p_c = p_{c1}p_{c2}$ for DLPs. Because of the general independence among the upper- and lower-level systems, as shown in Fig. 1(b), one might intuitively justify this conjecture as follows: If an infinite upper-level system is at criticality ($p_1 = p_{c1}$), it will percolate for the first time, and so do all infinite lower-level systems at criticality ($p_2 = p_{c2}$). Then the corresponding infinite DLP

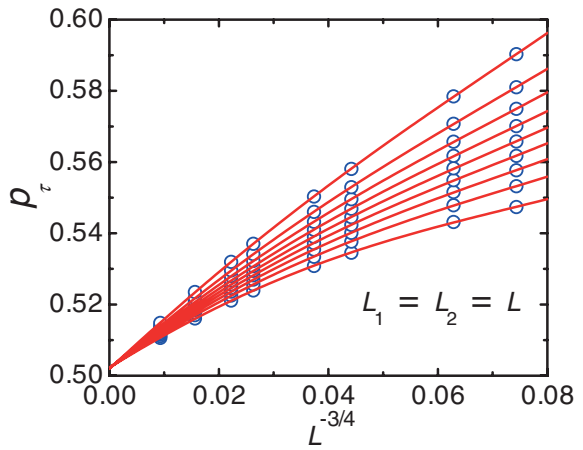

FIG. 6. (Color online) Plots of percolation threshold estimates $p_\tau(L)$ against $L^{-1/v}$ for the 1D-bond:2D-bond DLP with $L_1 = L_2 = L$. The curves are nonlinear regression fittings by Eq. (1) with $M = 2$ and $v = 4/3$. From bottom to top, τ increases from 0.1 to 0.9 in steps of 0.1.

TABLE IV. Extracted p_c for the 1D-bond:2D-bond DLP from the nonlinear fittings ($M = 2$) of Eq. (1) to different p_τ in Fig. 6. All the fittings have adjusted $R^2 > 0.9999$.

τ	p_c
0.1	0.50231(66)
0.2	0.50225(64)
0.3	0.50220(63)
0.4	0.50218(59)
0.5	0.50217(59)
0.6	0.50214(58)
0.7	0.50213(51)
0.8	0.50207(51)
0.9	0.50195(52)

is expected to percolate for the first time when $p = p_1p_2 = p_{c1}p_{c2}$.

Rigorously, however, the analysis in this work establishes that $p_c = 0.25177 \pm 0.00031$ is definitely larger than $p_{c1}p_{c2} = 0.25$. Similar characteristics are also observed for the other two DLPs: $p_c = 0.2975(5) > p_{c1}p_{c2} = 0.5 \times 0.59274621 = 0.296373105$ [16] for the 2D-bond:2D-site DLP, and $p_c = 0.5022(8) > p_{c1}p_{c2} = 1 \times 0.5 = 0.5$ [3] for the 1D-bond:2D-bond DLP.

It is interesting to explore the reason why p_c deviates from $p_{c1}p_{c2}$ in DLPs. The classical SLP theory does not offer an intuitive explanation of such "p_c deviation" in DLPs. Here, we offer three perspectives meant to encourage

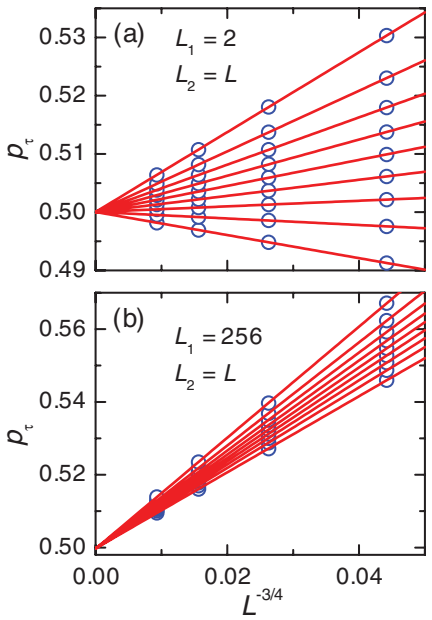

FIG. 7. (Color online) Plots of percolation threshold estimates $p_\tau(L)$ against $L^{-1/v}$ for the 1D-bond:2D-bond DLP with $L_2 = L$ ($L = 64$, 128, 256, and 512) and fixed L_1 (i.e., elongated 2D bond SLP). The curves are linear regression fittings by Eq. (1) with $M = 0$ and $v = 4/3$. From bottom to top, τ increases from 0.1 to 0.9 in steps of 0.1. In (a), $L_1 = 2$ and the estimated (average) $p_c = 0.50004 \pm 0.00012$. In (b), $L_1 = 256$ and the estimated (average) $p_c = 0.4997 \pm 0.0004$. Here, the uncertainties bracket the maximum uncertainties of all p_c estimations from different p_τ.

additional analytical work in this new class of DLP systems. First, a DLP can be equivalently viewed as sub-elements randomly deposited on a fractal space defined by the percolating clusters of super-elements. The fractal space is characterized by reduced (fractal) dimensionality $D_F \approx 1.9$ [3]. It is well known that p_c increases with decreasing D_F for finite-size fractal systems [23,24]. Therefore since $p_c = p_{c1}(D_F = 2)p_{c2}(D_F < 2) > p_{c1}(D_F = 2)p_{c2}(D_F = 2)$, the deviation may reflect reduced fractal space for the sub-elements.

For the second perspective, the percolating clusters of super-bonds contain "red bonds," single links in the clusters [25,26]. The DLP spanning requires that such red super-bonds must always be percolated (through sub-bonds) *with probability 1*, which might also result in the p_c increase.

For the third perspective, note that at infinity ($L_1 \to \infty$ and $L_2 \to \infty$), a DLP can be viewed as an infinite cluster [3,27] of super-elements populated by infinite clusters of sub-elements. Since the cluster size of super-elements is already infinite, probably the DLP system can percolate only if all infinite sub-element clusters exist with probability 1. In order to understand this point, it is important to appreciate the difference between elongated SLP and the 1D-bond:2D-bond DLP, as discussed in Sec. III C. Note that $p_c = p_{c1}p_{c2}$ in the case of elongated SLP (L_1 is fixed and only $L_2 \to \infty$, Fig. 7), whereas, $p_c > p_{c1}p_{c2}$ in the case of DLP (both $L_1 \to \infty$ and $L_2 \to \infty$, Fig. 6). Here we provide a plausible explanation for such a difference. Suppose, when $L_2 \to \infty$ and $p_2 = p_{c2}$, the spanning probability of the lower-level systems is R_c. In general, one may expect $0 < R_c < 1$. For an elongated SLP ($r = L_1$ is finite), its overall spanning probability is $\pi = R_c^{L_1}$, which in theory is definitely larger than 0, no matter how large L_1 is. We can therefore still expect the elongated SLP spans at $p_2 = p_{c2}$ since $\pi = R_c^{L_1} > 0$. However, for DLPs, at infinity, the overall spanning probability is $\pi = R_c^{L_1} = 0$ since $L_1 = \infty$. This is consistent with Cardy's formula for the spanning (crossing) probability of rectangular systems (elongated SLP), which also predicts that $\pi = 0$ when $r = \infty$ [21,22]. Then, we cannot expect the DLP to span at $p_2 = p_{c2}$, unless $R_c = 1$ with probability 1. However, the classical SLP theory suggests that no infinite cluster exists with probability 1 at criticality (at least when the dimensionality $d = 2$ or $d \geqslant 19$) [27,28]; they only exist when p_2 is strictly larger than p_{c2}. Therefore, the global p_c must necessarily be larger than $p_{c1}p_{c2}$.

The "p_c deviation" of DLP may therefore open up opportunities to reconsider a series of percolation problems concerning infinite clusters. The infinite cluster is an interesting, but not well studied, topic in SLP [3,28,29]. For instance, for dimensionalities $2 < d < 19$, the existence of infinite clusters at criticality is still an open question [28]. The p_c deviation in DLPs may provide an alternative perspective for this question.

Specifically, for example, let us ask "if an infinite cluster exists at criticality for $d = 3$." To answer this question, let us define a 1D-bond (line-like lattice, upper level):three-dimensional (3D)-bond (simple cubic lattice, lower level) DLP. Because of the unknown exact value of υ for 3D systems [17], instead of Eq. (1), we estimate p_c of such a DLP from $p_{\rm av} - p_c \propto \Delta$ [3,30], where $p_{\rm av} = \langle p \rangle$ is the average occupation probability at which DLP spanning first occurs, and $\Delta = \sqrt{\langle (p - p_{\rm av})^2 \rangle}$ is the root mean square deviation. Based on our algorithm, $p_{\rm av}$ and Δ can be readily calculated using a canonical method [19]. As shown in Fig. 8, this DLP has $p_c = 0.24971(39)$ [Fig. 8(b)], still definitely larger than $p_{c1}p_{c2} = 1 \times 0.248835(48) = 0.248835(48)$ [Fig. 8(a)], suggesting that for $d = 3$, *there are still no infinite clusters existing with probability 1 at criticality*. It should be straightforward to extend such investigations to other dimensionalities. From this perspective, the framework of DLP may not only be important for applications in nanoscience and nanotechnology, but also suggest an alternative approach to explore fundamental questions related to SLP, which cannot be easily answered within the SLP framework.

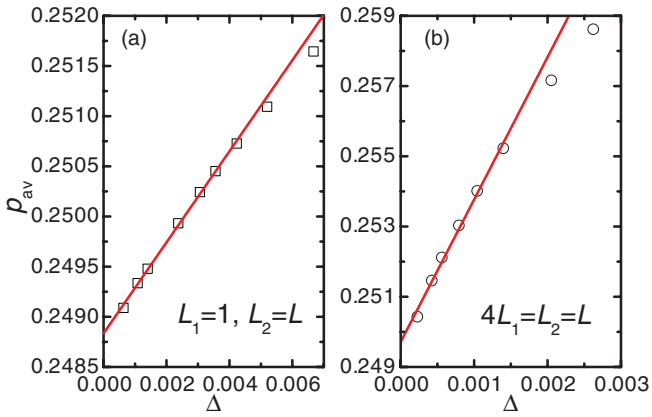

FIG. 8. (Color online) Plots of $p_{\rm av}$ versus Δ for the 1D-bond:3D-bond DLP (simple cubic lattice) DLP. (a) $L_1 = 1$ (fixed) and $L_2 = L$, which actually degrades to 3D SLP. (b) $4L_1 = L_2 = L$. L varies between 40 and 256. Each data point is based on $10^3 - 10^6$ samples. The linear fittings (adjusted $R^2 > 0.99$) give $p_c = 0.248835 \pm 0.000048$ for SLP in (a) and $p_c = 0.24971 \pm 0.00039$ for DLP in (b). In both fittings, the rightmost two points are not included.

V. CONCLUSION

In summary, this work introduces the concept of double-level percolation (as a special case of a hierarchical percolating system), which has promising applications in the emerging nanomaterials science and nanotechnology, and may also represent an important direction for the development of the classical single-level percolation theory. Large scale Monte Carlo simulations on multiple systems have indicated that double-level percolation threshold is close to, but strictly larger than, the product of the local percolation thresholds for the two enclosed single-level systems. Studies on such deviations may offer insights into fundamental physics concerning infinite clusters, which can further extend the theoretical applications of double-level percolation.

ACKNOWLEDGMENTS

J.L. and M.Ö. acknowledge the financial support by the Advanced Investigator Grant (OSIRIS, Grant No. 228229) from the European Research Council and the 7th Framework Program (NANOFUNCTION, NoE 257375) from the European Commission. B.R. and M.A.A. acknowledge support

from the Center for Re-Defining Photovoltaic Efficiency through Molecule Scale Control, an Energy Frontier Research Center funded by the US Department of Energy, Office of Science, Office of Basic Energy Sciences under Award No. DE-SC0001085 and the FRCP Center on Materials, Structures, and Devices.

[1] K. M. Golden, S. F. Ackley, and V. I. Lytle, Science **282**, 2238 (1998).
[2] Q. Cao *et al.*, Nature **454**, 495 (2008).
[3] D. Stauffer and A. Aharony, *Introduction to Percolation Theory*, 2nd revised ed. (Taylor and Francis, London, 2003).
[4] G. E. Pike and C. H. Seager, Phys. Rev. B **10**, 1421 (1974).
[5] J. Li and S.-L. Zhang, Phys. Rev. E **80**, 040104(R) (2009).
[6] C. R. Scullard and R. M. Ziff, Phys. Rev. Lett. **100**, 185701 (2008).
[7] A. Haji-Akbari and R. M. Ziff, Phys. Rev. E **79**, 021118 (2009).
[8] O. Riordan and L. Warnke, Science **333**, 322 (2011).
[9] M. Sumita *et al.*, Colloid. Polym. Sci. **270**,134 (1992).
[10] K. Levon, A. Margolina, and A. Z. Patashinsky, Macromolecules **26**, 4061 (1993).
[11] Such systems were previously called double percolation or multiple percolation [9,10]. However, these terms are more compatible with multiple independent percolations constructed by different components in a composite system [e.g., X. Liu *et al.*, Phys. Rev. Lett. **104**, 035701 (2010); C. Zhang *et al.*, Phys. Rev. B **71**, 014408 (2005)]. The nomenclature, double-level and/or multilevel percolation, can appropriately describe the hierarchical characteristics and effectively eliminate any ambiguity.
[12] K. Na *et al.*, Science **333**, 328 (2011).
[13] L. J. Cote, F. Kim, and J. Huang, J. Am. Chem. Soc. **131**, 1043 (2009).
[14] P. Y. Huang *et al.*, Nature **469**, 389 (2011).
[15] V. V. Cheianov, V. I. Fal'ko, B. L. Altshuler, and I. L. Aleiner, Phys. Rev. Lett. **99**, 176801 (2007).
[16] M. E. J. Newman and R. M. Ziff, Phys. Rev. Lett. **85**, 4104 (2000).
[17] M. E. J. Newman and R. M. Ziff, Phys. Rev. E **64**, 016706 (2001).
[18] P. M. C. de Oliveira, R. A. Nóbrega, and D. Stauffer, Braz. J. Phys. **33**, 616 (2003).
[19] R. M. Ziff and M. E. J. Newman, Phys. Rev. E **66**, 016129 (2002).
[20] As shown in Fig. 1(b), all the lower-level lattices are independent from one another. It is therefore not really necessary to set up a huge DLP lattice like Fig. 1(b). Instead, one can set up N_b independent lower-level lattices and attach each to one backbone super-bond. For more efficiency, before token allocation, we set up only one lower-level lattice and populate it for N_b runs. Each run produces a minimum sub-bond number N_{sub} needed for the lower-level lattice spanning [continuous path(s) connecting its two opposite local boundaries], and each N_{sub} is attached to one backbone super-bond. Then, during the token allocation, we do not need to populate any low-level lattices. A backbone super-bond is regarded to be percolated when it can collect no less than N_{sub} tokens. The DLP spans when the percolated (instead of occupied) super-bonds can form at least one cluster to connect the two opposite global boundaries.
[21] J. L. Cardy, J. Phys. A **25**, L201 (1992).
[22] R. M. Ziff, J. Phys. A **28**, 1249 (1995).
[23] Y. Bo-Ming and Y. Kai-Lun, Z. Phys. B **70**, 209 (1988).
[24] M. C. Sukop, G.-J. V. Dijk, E. Perfect, and W. K. P. V. Loon, Transp. Porous Media **48**, 187 (2002).
[25] B. H. Kaye, *A Random Walk through Fractal Dimensions*, 2nd ed. (Weinheim, New York, 1994).
[26] H. E. Stanley, J. Phys. A **10**, L211 (1977).
[27] H. Kesten, Probab. Theor. Relat. Fields **73**, 369 (1986).
[28] G. Grimmett, *Percolation* (Springer, Berlin, 1999).
[29] J. T. Chayes, L. Chayes, and R. Durrett, J. Phys. A **20**, 1521 (1987).
[30] D. Stauffer, J. Adler, and A. Aharony, J. Phys. A **27**, L475 (1994).